

# Photoactive Chiral Metal–Organic Frameworks for Light-Driven Asymmetric $\alpha$ -Alkylation of Aldehydes

Pengyan Wu, Cheng He,\* Jian Wang, Xiaojun Peng, Xuezhao Li, Yonglin An, and Chunying Duan\*

State Key Laboratory of Fine Chemicals, Dalian University of Technology, Dalian 116012, People's Republic of China

**S** Supporting Information

**ABSTRACT:** Chiral metal–organic frameworks (MOFs) with porous and tunable nature show promise as heterogeneous asymmetric catalysts. Through incorporating the stereoselective organocatalyst *L*- or *D*-pyrrolidin-2-ylimidazole (PYI) and a triphenylamine photoredox group into a single framework, we have developed two enantiomeric MOFs, Zn–PYI1 and Zn–PYI2, to prompt the asymmetric  $\alpha$ -alkylation of aliphatic aldehydes in a heterogeneous manner. The strong reductive excited state of the triphenylamine moiety within these MOFs initiated a photoinduced electron transfer, rendering an active intermediate for the  $\alpha$ -alkylation. The chiral PYI moieties acted as cooperative organocatalytic active sites to drive the asymmetric catalysis with significant stereoselectivity. Control experiments using the lanthanide-based metal–organic frameworks Ho–TCA and MOF–150, assembled from 4,4',4''-nitritotribenzoic acid, as catalysts suggested that both the photosensitizer triphenylamine moiety and the chiral organocatalyst *D*-/*L*-PYI moiety were necessary for the light-driven  $\alpha$ -alkylation reactions. Further investigations demonstrated that the integration of both photocatalyst and asymmetric organocatalyst into a single MOF makes the enantioselection superior to that of simply mixing the corresponding MOFs with the chiral adduct. The easy availability, excellent stereoselectivity, great separability, and individual components fixed with their well-defined porous and repeating structures make the MOF a versatile platform for a new type of tandem catalyst and cooperative catalyst.



## INTRODUCTION

Catalysis is at the heart of chemistry and provides tools for efficiently and selectively making and breaking chemical bonds that are crucial for converting basic chemicals into useful products for society in a sustainable fashion.<sup>1,2</sup> The observation that light alone could affect unique chemical changes in organic compounds led early 20th century photochemists to recognize that the sun might represent an inexhaustible source of clean chemical potential.<sup>3–6</sup> Building on the seminal results by employing photoinduced electron transfer processes, a variety of methods have been developed recently by applying organometallic complexes such as [Ru(bpy)<sub>3</sub>]<sup>2+</sup> and [Ir(ppy)<sub>2</sub>(dtb-bpy)]<sup>+</sup> (bpy = bipyridine, ppy = 2-phenylpyridine, dtb-bpy = 4,4'-di-*tert*-butyl-2,2'-bipyridine).<sup>7–10</sup> Of particular interest is the cooperative combination of a photocatalyst with an organo-catalytic cycle, offering one of the rare catalytic methods for the  $\alpha$ -alkylation of aldehydes.<sup>11–13</sup> Like other precious-metal-catalyzed reactions, it is highly desirable to develop recyclable and reusable photocatalytic systems based on the metal–organic chromophores or more environmentally friendly organic dyes.<sup>14,15</sup> In particular, the ability to recover and reuse photocatalysts in a heterogeneous manner can not only eliminate the contamination of organic products by trace amounts of heavy metals but also reduce the processing and waste disposal costs in large-scale reactions.<sup>16,17</sup>

On the other hand, metal–organic frameworks (MOFs) are hybrid solids with infinite network structures built from organic bridging ligands and inorganic connecting points.<sup>18–20</sup> These materials have shown promise in catalysis, gas storage,

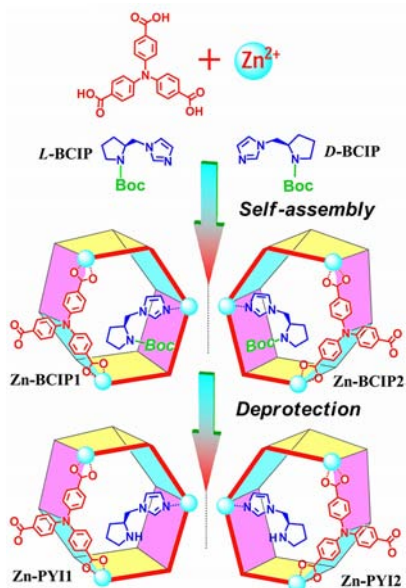
molecular sensing, separation, and medical applications.<sup>21–24</sup> In particular, chiral porous MOFs are ideally suited for heterogeneous asymmetric catalytic conversions because they impose size- and shape-selective restrictions through readily fine-tuned channels and pores<sup>25,26</sup> and high enantioselectivity through the imbedded, regularly ordered chiral functionalities.<sup>27</sup> The intrinsic crystalline properties also provided precise knowledge about the pore structure and the nature and distribution of catalytically active sites.<sup>28–30</sup> In comparison to the heterogeneous catalytic systems that have been examined earlier, the design flexibility and framework tenability resulting from the huge variations of metal nodes and organic linkers likely allow the introduction of two independent catalytic units into one well-defined MOF.<sup>31,32</sup> Especially, the incorporation of an asymmetric organocatalyst within a photoactive MOF might be an efficient approach to create new synergistic catalysts combining both photocatalytic and organocatalytic cycles.

By combining an easily prepared asymmetric organo-catalytic group, *L*- or *D*-pyrrolidine-2-ylimidazole (PYI), and a photoactive nitritotribenzoate building block within a single MOF, herein we report the design and synthesis of two new enantiomorphs of chiral MOFs, Zn–PYI1 and Zn–PYI2 (Scheme 1), which can perform light-driven asymmetric  $\alpha$ -alkylation of aliphatic aldehydes in a heterogeneous manner. We envisioned that the triphenylamine moiety in the MOF

Received: June 3, 2012

Published: August 13, 2012

**Scheme 1. Schematic Representation of the Mirror Image Structures of Zn–BCIP1 and Zn–BCIP2 and Their Deprotected Forms Zn–PYI1 and Zn–PYI2, Showing the Photosensitizer, 4,4',4''-Nitrilotribenzoic Acid (Red or Simply Drawn as Block Red Bars), and the Chiral Organocatalytic Moiety, L- or D-Proline Derivatives (Blue)**



likely worked as an electron donor to initiate a photoinduced single electron transfer from its excited state to the diethyl 2-bromomalonate,<sup>33–36</sup> a well-known  $\alpha$ -alkylation agent, rendering an active radical that potentially undergoes  $\sigma$ -bond cleavage to afford an active intermediate for the  $\alpha$ -alkylation of an aliphatic aldehyde.<sup>37</sup> In the meantime, the chiral PYIs would act as cooperative organocatalytic active sites, where a highly  $\pi$ -nucleophilic enamine combines with the electron-deficient radical to forge a crucial reaction center that drives the heterogeneous catalysis in an asymmetric manner,<sup>37–40</sup> as used in asymmetric aldol reactions and other asymmetric transformations.<sup>41</sup>

## RESULTS AND DISCUSSION

The solvothermal reaction of 4,4',4''-tricarboxyltriphenylamine ( $H_3TCA$ ) and  $Zn(NO_3)_2 \cdot 6H_2O$  in the presence of *L-N*-tert-butoxycarbonyl-2-(imidazole)-1-pyrrolidine (*L*-BCIP)<sup>42</sup> in a mixed solvent of DMF and ethanol gave the compound Zn–BCIP1 in a yield of 60%. Elemental analyses along with powder X-ray analysis (XRD) indicated the pure phase of its bulk sample. Single-crystal X-ray structural analysis revealed that Zn–BCIP1 crystallizes in the chiral space group  $P2_1$ . It has a two-dimensional brick wall layered structure built from three-connected binuclear zinc nodes and 4,4',4''-nitrilotribenzoate bridges (Figure 1). In each binuclear unit, one of the Zn atoms is coordinated by five oxygen atoms from one bridged hydroxyl anion, one water molecule, and one bidentate and one bimonodentate carboxylate group of two different  $TCA^{3-}$  anions, resulting in a distorted-trigonal-bipyramidal geometry. Another zinc atom is coordinated in a distorted-tetrahedral geometry with two carboxylate oxygen atoms from different  $TCA^{3-}$  anions, one bridged hydroxyl anion, and one nitrogen atom from the *L*-BCIP ligand, respectively. The adjacent layer is stacked face to face with pairs of *L*-BCIP located within the cavities, ensuring the chirality of the whole layer. These bilayer

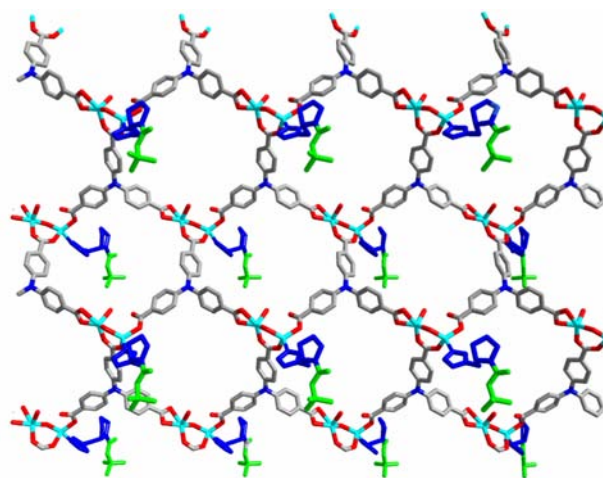


**Figure 1.** Crystal structure of Zn–BCIP1 showing the two-dimensional sheet constructed by 4,4',4''-nitrilotribenzoic acid and zinc ions and the chiral organocatalytic moiety, *L*-proline derivative, positioned within the cavities as well as the fragments of the MOF including the light-harvesting groups (gray), the chiral organocatalyst unit (blue), the removable Boc moiety (green), and the metal centers (cyan).

structures further align parallel to each other, completing the packing pattern and forming 1D channels of  $12 \times 16 \text{ \AA}^2$  viewed along the [100] direction (Scheme 1). *L*-BCIP molecules locate within the channels with the potential catalytically active site N–H of pyrrolidine protected by the *tert*-butoxycarbonyl (Boc) group. The use of the thermolabile Boc as the starting material for the MOF synthesis can protect the pyrrolidine moiety and preclude framework interpenetration, producing open frameworks with the vacant space adjacent to the catalytic units.<sup>43,44</sup>

Thermogravimetric analysis (TGA) of Zn–BCIP1 exhibited a significant weight loss of 12.9%, approximately corresponding to one Boc moiety per triphenylamine group in the region 100–200 °C, suggesting that the thermolytic reaction of the Boc moiety was possibly taking place within this temperature range. Deprotection of the proline unit was accomplished by simply heating as-synthesized Zn–BCIP1 in a dry *N,N*-dimethylformamide solution using microwave irradiation to generate the new compound Zn–PYI1 in a postsynthetic fashion (Figure 2).<sup>43–46</sup> The expulsion of the Boc group was further verified by <sup>1</sup>H NMR of the MOF crystals digested in  $DMSO-d_6/DCI$  and IR spectra. The phase purity of Zn–PYI1 was established by powder X-ray diffraction. The observed diffraction pattern closely matched that of Zn–BCIP1, evidencing the maintenance of crystallinity.

Dye-uptake studies were carried out by soaking Zn–PYI1 in a methanol solution containing 2',7'-dichlorofluorescein for 12 h. After the soaked Zn–PYI1 was washed with solvent several times to remove dye molecules adsorbed on the external surfaces of the crystals, the dye-loaded Zn–PYI1 was then digested with sodium ethylenediaminetetraacetic acid. The amounts of released 2',7'-dichlorofluorescein were quantified by ultraviolet–visible spectroscopy and demonstrated an uptake equivalent to as much as 14% of the framework weight.<sup>47,48</sup> Since the as-synthesized Zn–BCIP1 did not exhibit any obvious dye uptake, these results clearly implied the releasing of channels during the deprotection process. In this case, the dye uptake experiment also demonstrated conclusively the

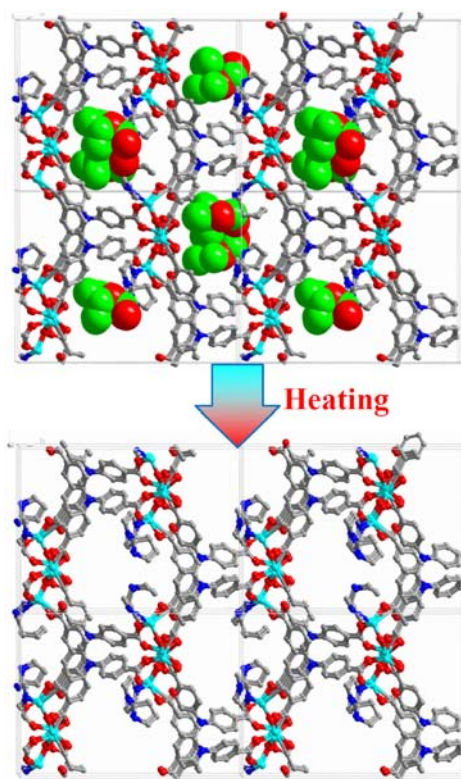


**Figure 2.** Crystal structure of the multifunctional framework Zn-BCIP1 showing the packing pattern of these layers (top) and the simulated structure of Zn-PYI1 obtained by thermolytic expulsion of the Boc moieties (bottom), showing the enlargement of the porous MOFs within the channels. The cyan, red, blue, gray, and green balls represent the Zn, O, N, and C atoms and Boc moiety, respectively.

accessibility of the potential actively catalytic sites to the organic substrates through the open channels.

Circular dichroism (CD) spectrum of Zn-BCIP1 exhibited a positive Cotton effect at about 260 nm and a negative Cotton effect centered at 330 nm (Figure 3). The spectrum was quite different from that of L-BCIP. The peak at 330 nm was assignable to the absorbance difference corresponding to the  $\pi-\pi^*$  transition of the triphenylamine groups.<sup>49–51</sup> This result might be one of the indicators for the homochirality of the whole framework. Moreover, CD spectroscopy of Zn-PYI1 showed a negative Cotton effect centered at 345 nm and a positive Cotton effect at about 245 nm, indicating the maintenance of chirality from Zn-BCIP1 to Zn-PYI1.

UV-vis absorption spectrum of Zn-PYI1 in the solid state exhibited an absorption band centered at 350 nm typically assignable to the  $\pi-\pi^*$  transition of the triphenylamine group.<sup>49–51</sup> Upon excitation at this absorption band, Zn-PYI1 showed an intense luminescence band at about 450 nm, as reported in the related compounds.<sup>52</sup> Solid-state electrochemical measurements exhibited a redox potential at 0.84 V (vs SCE), assignable to the redox potential of the Zn-PYI1<sup>+</sup>/Zn-PYI1 couple (Figure 4). The redox potential of the excited-state Zn-PYI1<sup>+</sup>/Zn-PYI1\* couple was calculated as -2.12 V on the basis of a free energy change ( $E^{0-0}$ ) between the ground state and the vibrationally related excited state of 2.96 eV.<sup>53,54</sup> This potential was comparable to that of the excited state *fac*-Ir(ppy)<sub>3</sub>\* in an acetonitrile solution and was more negative than that of the diethyl 2-bromomalonate ( $E^0 = -0.49$  V).<sup>11,37</sup> As a consequence, Zn-PYI1 was considered to

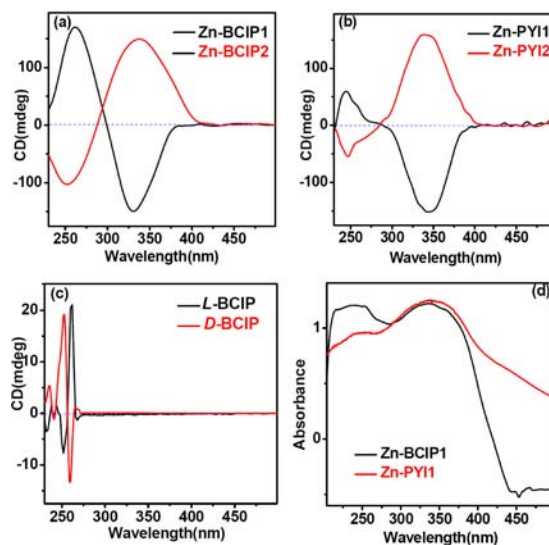


**Figure 3.** (a) Circular dichroism spectra of bulk crystals of Zn-BCIP1 and Zn-BCIP2. (b) Circular dichroism spectra of bulk crystals of Zn-PYI1 and Zn-PYI2. (c) Circular dichroism spectra of L-BCIP and D-BCIP in DMF solution. (d) UV-vis absorption spectra of Zn-BCIP1 and Zn-PYI1 in the solid state.

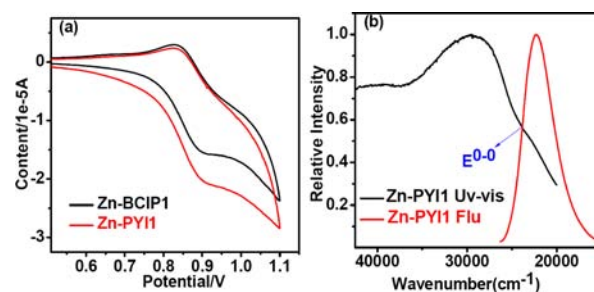


**Figure 4.** (a) Solid-state CV of Zn-BCIP1 and Zn-PYI1 with a scan rate of 50 mV s<sup>-1</sup> in the scan range 0.5–1.1 V. (b) Normalized absorption (black line) and emission spectra (red line) of Zn-PYI1, excited at 350 nm.

be a candidate for the photocatalysis of the alkylation reaction of the aldehydes coupled with diethyl 2-bromomalonate.

The pores of Zn-PYI1 showed adsorption ability toward phenylpropylaldehyde or diethyl 2-bromomalonate, the possible substrates for asymmetric  $\alpha$ -alkylation. As-synthesized Zn-PYI1 was immersed in CH<sub>2</sub>Cl<sub>2</sub> containing each reagent, phenylpropylaldehyde or diethyl 2-bromomalonate, respectively. The powder was filtered off and dried in air, and then its <sup>1</sup>H NMR and IR spectra were acquired. <sup>1</sup>H NMR of Zn-PYI1 adsorbed the substrates digested in DMSO-*d*<sub>6</sub>/DCl demonstrated that Zn-PYI1 could adsorb about 1 equiv of phenylpropylaldehyde per proline moiety. IR of the catalyst impregnated with a CH<sub>2</sub>Cl<sub>2</sub> solution of phenylpropylaldehyde revealed a C=O stretching vibration at 1715 cm<sup>-1</sup> for phenylpropylaldehyde included in Zn-PYI1. The red shift from 1724 cm<sup>-1</sup> (free aldehyde) suggested the adsorption and the activation of the aldehyde in the channels of the MOFs, through the interactions between Zn-PYI1 and the C=O group of the aldehyde, possibly giving a highly  $\pi$ -nucleophilic enamine.

An absorption experiment also demonstrated that Zn-PYI1 could also adsorb 1.5 molecular stoichiometric amounts of diethyl 2-bromomalonate per triphenylamine moiety. Notice-

ably, the luminescence intensity of Zn–PY11 was significantly reduced when it absorbed diethyl 2-bromomalonate molecules (Figure 5).<sup>55</sup> Luminescence decays at 450 nm for Zn–PY11

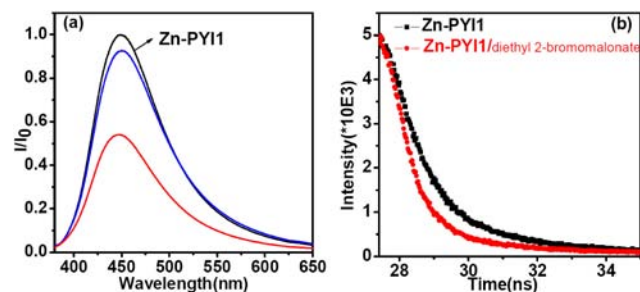


**Figure 5.** (a) Solid-state emission spectra of Zn–PY11 (black line), Zn–PY11 upon absorbance of phenylpropylaldehyde (blue line) and diethyl 2-bromomalonate (red line), excited at 350 nm. (b) Transient emission spectra of solid Zn–PY11 and Zn–PY11 with diethyl 2-bromomalonate incorporated.

exhibited a biexponential fashion with the lifetime calculated as 2.36 ns. The decrease of fluorescence lifetime of Zn–PY11 adsorbed diethyl 2-bromomalonate (1.51 ns) suggested the occurrence of a photoinduced electron transfer process from Zn–PY11\* to the diethyl 2-bromomalonate molecules. However, the adsorbance of phenylpropylaldehyde hardly quenched the luminescence significantly under the same experimental conditions. These results demonstrated that the quenching process was typically attributed to the photoinduced electron process from Zn–PY11\* to diethyl 2-bromomalonate, enhancing the possibility of occurrence of light-induced  $\alpha$ -alkylation of aldehydes.<sup>56,57</sup>

As shown in Table 1, the transformation was examined initially by using phenylpropylaldehyde and diethyl 2-

**Table 1. Conversions and ee Values (in Parentheses) of the Photocatalytic  $\alpha$ -Alkylation of Aliphatic Aldehydes**

		$\text{H}-\text{C}(\text{R})-\text{CHO} + \text{Br}-\text{C}(\text{CO}_2\text{Et})_2 \xrightarrow[0.5\text{mol}\% \text{catalyst}]{\text{fluorescent lamp}} \text{H}-\text{C}(\text{R})-\text{C}(\text{CO}_2\text{Et})_2$		
Entry	Catalyst			
Zn–PY11 <sup>a</sup>		74(+92)	65(+86)	84(+92)
Zn–PY12 <sup>a</sup>		73(-81)	61(-78)	85(-89)
Ho–TCA/L–PY1 <sup>b</sup>		86(+20)	90(+21)	93(+20)
Ho–TCA/D–PY1 <sup>b</sup>		85(-21)	90(-20)	95(-20)
MOF–150/L–PY1 <sup>b</sup>		67(+21)	78(+24)	80(+20)
MOF–150/D–PY1 <sup>b</sup>		62(-22)	73(-22)	80(-21)

<sup>a</sup>Reaction conditions: diethyl 2-bromomalonate, 0.385 mmol; aliphatic aldehyde, 0.769 mmol; 2,6-lutidine, 0.769 mmol; catalyst, 1.9  $\mu\text{mol}$  (0.5 mol %) per triphenylamine moiety; 26 W fluorescent lamp, room temperature under  $\text{N}_2$  for 24 h. <sup>b</sup>In the presence of additional chiral D-/L–PY1 (76.9  $\mu\text{mol}$ ).

bromomalonate as the coupling partners, along with Zn–PY11 and a common fluorescent lamp (26 W) as the light source. The results revealed the successful execution of our MOF design, showing a high reaction efficiency (74% in yield) and excellent enantioselectivity (92% ee). Other substrates (e.g., octaldehyde and (*E*)-non-6-enal) were also found to be prone to react with diethyl 2-bromomalonate under these mild

redox conditions. Zn–PY11 thus represents the first example of an MOF-based heterogeneous asymmetric photocatalyst for this important reaction, making a MOF a versatile platform for a new type of tandem catalyst and cooperative catalyst.

A number of control experiments were carried out to unveil the heterogeneous and photocatalytic nature of the reactions. A reaction set in the dark yielded negligible amounts of the  $\alpha$ -alkylation product, manifesting the necessity of light for this reaction. The use of Zn–BCIP1 instead of Zn–PY11 as the catalyst could not prompt the reaction, possibly due to either the poor porosity of Zn–BCIP1 or the low activating ability of the protected amine moiety toward the substrates. In addition, the removal of Zn–PY11 by filtration after 12 h shut down the reaction, affording only 5% additional conversion upon stirring for another 12 h. These experiments demonstrate that Zn–PY11 is a true heterogeneous catalyst.<sup>58</sup> It is also quite significant that solid Zn–PY11 can be easily isolated from the reaction suspension by simple filtration alone and can be reused at least three times with a slight decrease in its reactivity and selectivity (yield decreasing from 74% to 70% with the ee value decreasing from 92% to 88%). The index of XRD patterns of the Zn–PY11 bulk sample filtered off from the catalytic reaction evidence the maintenance of the framework. Also, the dye uptake study on the recovered catalysts exhibited almost same uptake ability (13%) for 2',7'-dichlorofluorescein, comparable with that of its original form.

The smooth reaction between diethyl 2-bromomalonate and phenylpropylaldehyde, octaldehyde, or (*E*)-non-6-enal, respectively, suggested that the window size of the catalyst is large enough to allow these substrates to pass through (Table 2).

**Table 2. Molecular Size of Aliphatic Aldehyde Substrates for  $\alpha$ -Alkylation<sup>a</sup>**

substrate	Molecular size
1a	
1b	
1c	
1d	

<sup>a</sup>The assumed structures and the molecular size were calculated by using the program Chem3D.<sup>61,62</sup>

However, in the presence of bulky aldehyde **1d**,<sup>59,60</sup> whose size is larger than the pore size of Zn–PY11 as the aldehyde substrate, the photocatalytic  $\alpha$ -alkylation reaction only gave 7% of product under the same reaction conditions. The size selectivity of the substrate suggested that the alkylation reactions occurred mostly in the channel of the catalyst, not on the external surface. Further adsorption experiments by immersing Zn–PY11 into a solution of **1d** also confirmed that the substrate **1d** was too large to be adsorbed in the channels of the MOF.

Similarly, the use of D–BCIP resulted in the formation of another enantiomorph, Zn–BCIP2. Zn–BCIP2 crystallizes in the chiral space group  $P2_1$  with cell dimensions similar to those

of Zn-BCIP1. The CD spectrum of Zn-BCIP2 exhibited Cotton effects opposite to those of Zn-BCIP1, as expected for a pair of enantiomers with a mirror-image relationship between each other.<sup>63,64</sup> Also, the photoactive MOF Zn-PYI2 was obtained by the same synthetic procedure. The solids of the catalysts with Cotton effects opposite to those of Zn-PYI1 exhibited similar catalytic activities but gave different products with opposite chiralities in the alkylation reaction of aldehydes with diethyl 2-bromomalonate. This implies that our approach could benefit the design and synthesis of efficient asymmetric catalysts for producing chiral fine chemicals and pharmaceuticals, where enantiomorphs with different chiralities manifest differentiation in their optical properties and biological activities.<sup>65</sup>

Similar to the case for *fac*-Ir(ppy)<sub>3</sub><sup>+</sup> in the photocatalysis reaction,<sup>37</sup> the excited state of triphenylamine could act as a reductant in the single electron transfer reaction from Zn-PYI1\* to diethyl 2-bromomalonate that renders a radical anion. According to a discussion on the mechanism of the photocatalysis reaction,<sup>37</sup> the resulting radical anion rapidly undergoes  $\sigma$ -bond cleavage to afford the bromide anion and an electrophilic radical. Within the same time frame, the condensation of an aldehyde substrate with N-H of a proline-based catalyst likely gives a highly  $\pi$ -nucleophilic enamine which then combines with the electron-deficient radical to forge a crucial reaction center. Consequently, the rapid oxidation of the resulting amino radical by Zn-PYI1<sup>+</sup> would then close the redox cycle and regenerate the photocatalyst Zn-PYI1.<sup>11,66</sup>

To further investigate the catalytic performance of MOFs containing light-harvesting triphenylamine groups, a new infinite 3D (6,3)-connected net with  $\mu_3$ -oxo-bridged Ho<sub>4</sub>(OH)<sub>4</sub> anamorphic cubic clusters as nodes and triphenylamine moieties as three-connected bridges was achieved via a solvothermal reaction using H<sub>3</sub>TCA and Ho(NO<sub>3</sub>)<sub>3</sub>·6H<sub>2</sub>O as the original reactants (Figure 6). Elemental analyses along with a powder X-ray analysis were indicative of the pure phase of its bulk sample. Ho-TCA crystallizes in the space group  $P\bar{4}2_1c$ . Single crystal structure analysis revealed that the topology of

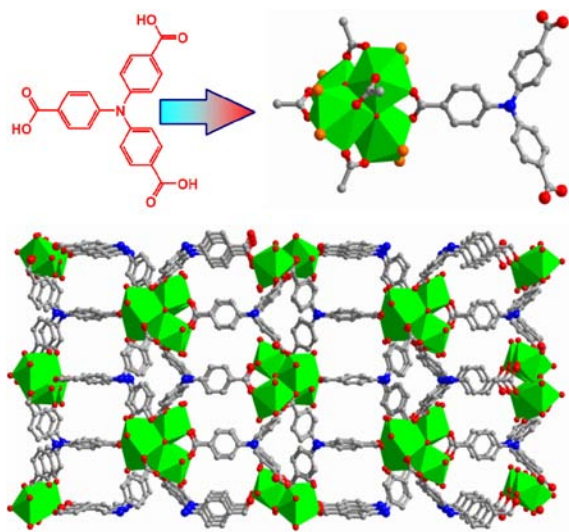


**Figure 6.** Synthetic approach of Ho-TCA (top) and its crystal packing along a direction showing the channels with metal ions and photoactive moieties exposed (bottom).

Ho-TCA was similar to that of the porous metal-organic framework MOF-150, a MOF assembled from zinc ions and 4,4',4''-nitrilotribenzoic acid, which was used for control reactions (vide infra).<sup>67</sup> The secondary building unit (SBU) Ho<sub>4</sub>(OH)<sub>4</sub> cluster is composed of four Ho centers bridged by six carboxylate groups from six TCA<sup>3-</sup> ligands, and in turn each TCA<sup>3-</sup> ligand connects three Ho<sub>4</sub>(OH)<sub>4</sub> clusters to form a (6,3)-connected network. Each Ho ion is eight-coordinated by three  $\mu_3$ -bridged hydroxyl anions, three carboxyl oxygen atoms, and two water molecules. The 3D network structure of Ho-TCA can be viewed as a Pd<sup>2+</sup> net<sup>68</sup> or a FeS<sup>2-</sup> net<sup>69</sup> with sections of 15.0 × 17.8 Å<sup>2</sup>, which are large enough for the accommodation and exchange of the corresponding small guests.

The free volume for fully desolvated Ho-TCA was estimated to be ~58.6% by PLATON<sup>70</sup> software; TGA analyses also showed that Ho-TCA exhibited an impressive solvent weight loss of 10.5 wt % in the temperature range 50–200 °C, indicative of a stable open framework structure. Dye uptake studies exhibited a 23% uptake of 2,7-dichlorofluorescein corresponding to the framework weight, illustrating the accessibility of the MOF to small molecules. Solid-state UV-vis absorption and luminescence spectra of Ho-TCA exhibited the characteristic absorption band centered at 350 nm and emission band at about 435 nm. The blue shift of the emission band leading to higher energy of the excited state of the Ho-TCA is likely to give it better catalytic ability.

As-synthesized Ho-TCA was immersed in CH<sub>2</sub>Cl<sub>2</sub> solution containing diethyl 2-bromomalonate or phenylpropylaldehyde, respectively, and stirred. The powder was filtered off and dried in air. <sup>1</sup>H NMR spectra demonstrated that Ho-TCA could include about two molecular stoichiometric amounts of diethyl 2-bromomalonate per triphenylamine moiety or 1 equiv of phenylpropylaldehyde per holmium ion, respectively. The adsorption of diethyl 2-bromomalonate also quenched the luminescence of Ho-TCA significantly. Exponential decay profiles suggested a significant decrease of luminescence lifetime from 2.26 ns for free Ho-TCA to 1.16 ns for diethyl 2-bromomalonate adsorbed Ho-TCA (Figure 7). The presence of phenylpropylaldehyde hardly quenched the luminescence of Ho-TCA, either with or without the organocatalyst PYI. These results confirmed that the electron transfer event should occur between the excited state of the photosensitizer triphenylamine moiety and diethyl 2-bromo-

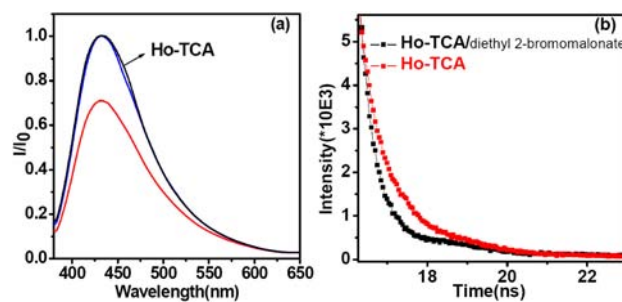


**Figure 7.** (a) Solid-state emission spectra of Ho-TCA upon adsorption of diethyl 2-bromomalonate (red line) or phenylpropylaldehyde and L-PYI (blue line), respectively. (b) Transient emission spectra of solid Ho-TCA and Ho-TCA upon absorption of diethyl 2-bromomalonate. The intensities were recorded at 435 nm, on excitation at 350 nm.

malonate, in accord with the proposed catalytic process mentioned above.

Solid state electrochemical measurements exhibited the redox potential  $E_{1/2}(\text{Ho-TCA}^+/\text{Ho-TCA})$  of 0.86 V (vs SCE) in the scan range 0.5–1.1 V (Figure 8). Accordingly, a redox

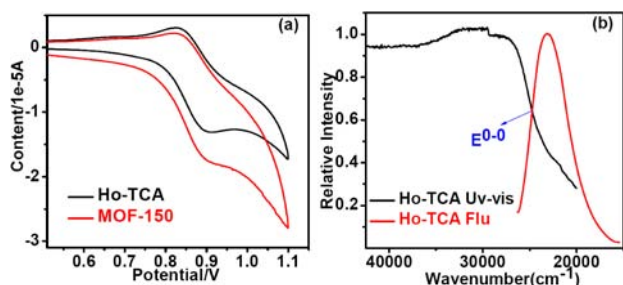


**Figure 8.** (a) Solid-state CV of Ho-TCA and MOF-150 with a scan rate of  $50 \text{ mV s}^{-1}$  in the range 0.5–1.1 V. (b) Normalized absorption (black line) and emission spectra (red line) of Ho-TCA, excited at 350 nm.

potential of  $-2.20 \text{ V}$  for that of the excited state  $E_{1/2}(\text{Ho-TCA}^+/\text{Ho-TCA}^*)$  was calculated according to a  $E^{0-0}$  of 3.06 eV obtained by the electronic spectra.<sup>53,54</sup> As mentioned above, this potential is negative enough to reduce diethyl 2-bromomalonate and is more negative than that of the redox potential of the excited state  $\text{Zn-PYI}^+/\text{Zn-PYI}^*$  couple; it is postulated that Ho-TCA possibly exhibits better catalytic effects for the  $\alpha$ -alkylation of aliphatic aldehyde.

As can be expected, reaction of phenylpropylaldehyde with diethyl 2-bromomalonate in the presence of 20 mol % of the secondary amine L-PYI as the organocatalyst with photocatalyst Ho-TCA afforded the  $\alpha$ -alkylation product with a yield of 86% and ee value of 20%. Importantly, removal of L-PYI from the standard protocol resulted in negligible alkylation product during the same time frame. The result demonstrated that L-PYI played an important role in activating the reaction substrates and was a necessary organocatalyst for this reaction.<sup>11</sup>  $^1\text{H}$  NMR of Ho-TCA immersed in L-PYI solution demonstrated that Ho-TCA could adsorb about 1 equiv of L-PYI per holmium ion (Figure 9); however, CD spectroscopy of

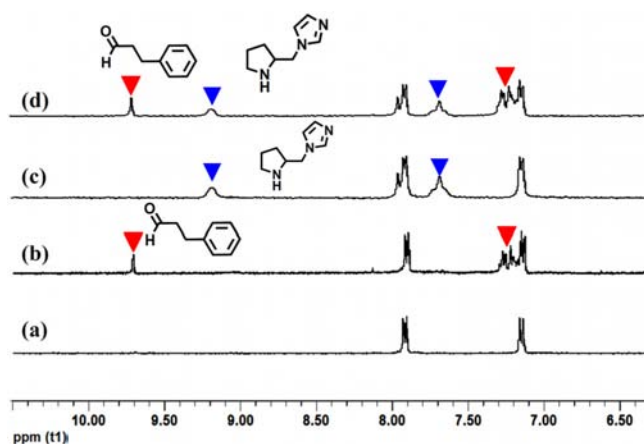


**Figure 9.**  $^1\text{H}$  NMR spectra of Ho-TCA (a), Ho-TCA adsorbed phenylpropylaldehyde (b), Ho-TCA adsorbed L-PYI (c), and Ho-TCA adsorbed phenylpropylaldehyde and L-PYI (d). Peaks marked with red triangles and blue triangles represent signals of phenylpropylaldehyde and L-PYI, respectively.

Ho-TCA adsorbed L-PYI did not show any obvious Cotton effect peaks corresponding to the triphenylamine groups, suggesting that its fragments were hardly positioned within a chiral environment. The immersion of Ho-TCA into a methanol solution containing a mixture of L-PYI and phenylpropylaldehyde for 12 h gave the solid of Ho-TCA containing 1 equiv of L-PYI and 1 equiv of phenylpropylaldehyde per holmium ion. This result suggested that L-PYI was likely to work as a chiral organocatalyst interacting with the aldehyde, possibly giving a highly  $\pi$ -nucleophilic enamine.<sup>11</sup>

Furthermore, the catalytic reactions were also size selective; replacing the aldehyde with the bulky aldehyde **1d** under the same reaction condition coupled with diethyl 2-bromomalonate only caused a negligible conversion of the products. The adsorption experiments also confirmed that the substrate **1d** was too large to be absorbed within the channels of the MOF Ho-TCA. The results also suggested that the reaction occurred mostly in the channel of the Ho-TCA. Solid Ho-TCA can be easily isolated from the reaction suspension by simple filtration alone and can be reused at least three times with a slight decrease in its reactivity and selectivity (yield decreasing from 86% to 84%). Similarly, the use of D-PYI resulted in the formation of another enantiomorph with similar conversions. For all the substrates, the obtained yields of the isolated products of entries 3 and 4 are better than that of entry 1 and entry 2 (Table 1), but the ee values are much lower than those for Zn-PYIs. The index of XRD patterns of the Ho-TCA bulk sample filtered off from the catalytic reaction evidences the maintenance of the framework. Also, the dye uptake study on the recovered catalysts exhibited almost the same uptake ability (24%) on 2',7'-dichlorofluorescein, in comparison with its original form. These experiments demonstrate that Ho-TCA is also a heterogeneous catalyst. The higher transformation efficiencies of Ho-TCA can likely be attributed to the more negative redox potentials of the excited states of the triphenylamine moiety. In addition, the much lower asymmetric selectivity of Ho-TCA can possibly be attributed to the absence of chiral environments.

At the same time, the previously reported MOF-150 (Figure 10), containing 4,4',4''-nitrotribenzoic acid as the building blocks, was also chosen as a comparison catalyst for the light-driven asymmetric  $\alpha$ -alkylation of aliphatic aldehydes. Diethyl 2-bromomalonate also considerably decreased the luminescence intensities of MOF-150 with a quenching efficiency of about 26%. Solid-state electrochemical measure-

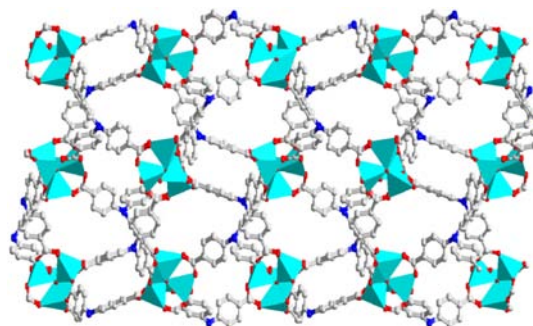


**Figure 10.** Crystal structure of MOF-150<sup>69</sup> along a direction showing the cavity channels with zinc acetate octahedral SBUs composed of four  $\text{ZnO}_4$  tetrahedra sharing a common corner and photoactive moieties exposed.

ments exhibited a redox potential at 0.85 V for MOF-150, from which the redox potential of the related excited state was calculated as  $-2.09$  V. These potentials are negative enough to reduce diethyl 2-bromomalonate, so that MOF-150 excited state might also behave as a reductant in the photoredox cycle. The reactions catalyzed by MOF-150 in the presence of additional chiral organo-catalyst *L*-/*D*-PYI produced alkylation products in good yields (62–80%) and low enantioselectivity (ee 20–22%), as shown in entries 5 and 6 of Table 1.

Both Ho-TCA and MOF-150 are effective photocatalysts for the  $\alpha$ -alkylation reaction between aldehydes and diethyl 2-bromomalonate, demonstrating that the triphenylamine fragment is the key component for photocatalytic activity. The different transformation efficiencies of the catalytic reactions can likely be attributed to the different redox potentials of the excited states of triphenylamine moieties in different environments as well as the luminescence quenching efficiencies related to the adsorbed diethyl 2-bromomalonate substrate. Interestingly, the ee values using Ho-TCA or MOF-150 as photocatalyst are much lower than that using Zn-PYIs, despite the fact that the same chiral adduct *L*-PYI (or *D*-PYI) was used in the reaction. Clearly, the integration of both photocatalyst and asymmetric organocatalyst into a single MOF makes the enantioselection superior to that of simply mixing the corresponding MOFs with the chiral adduct. Most likely this is due to the restricted movement of the substrates within the MOF's interior and multiple chiral inductions as well. The easy availability, excellent stereoselectivity, and great separability and also the individual components fixed with their well-defined porous and repeating structures make the MOF a versatile platform for a new type of tandem catalyst and cooperative catalyst.

## CONCLUSION

A new approach to obtain a MOF-based asymmetric photocatalyst through the cooperative combination of triphenylamine photocatalysis and proline-based asymmetric organocatalysis within a single MOF was developed. With their well-defined, repeating structures, the individual components are fixed in a structurally controlled manner, and the catalysts have been successfully applied to prompt the light-driven  $\alpha$ -alkylation reaction with excellent catalytic efficiency and high enantioselectivity.

## EXPERIMENTAL SECTION

**Material and Methods.** Unless otherwise stated, all chemical materials were purchased from commercial sources and used without further purification. 4,4',4''-Tricarboxytriphenylamine ( $H_3TCA$ )<sup>71</sup> and *L*-/*D*-*N*-*tert*-butoxycarbonyl-2-(imidazole)-1-pyrrolidine (*L*-/*D*-BCIP)<sup>42</sup> were synthesized according to the published procedures. <sup>1</sup>H NMR spectra were measured on a Varian INOVA 400 M spectrometer. Elemental analyses were obtained on a Vario EL III Elemental Analyzer. Powder XRD diffractograms were obtained on a Rigaku D/Max-2400 X-ray diffractometer with Cu sealed tube ( $\lambda = 1.54178$  Å). Thermogravimetric analysis (TGA) was carried out at a ramp rate of 5 °C/min in a nitrogen flow with a Mettler-Toledo TGA/SDTA851 instrument. FT-IR spectra were recorded as KBr pellets on JASCO FT/IR-430. Solid UV-vis spectra were recorded on a HP 8453 spectrometer. Liquid UV-vis spectra were performed on a TU-1900 spectrophotometer.

The solid fluorescent spectra were measured on a JASCO FP-6500 instrument. The excitation and emission slits were both 3 nm wide. Adding Zn-PYI (50 mg) to a dichloromethane solution containing substrates and stirring for 12 h afforded new crystalline solids; the

intensity was recorded at 450 nm, and excitation was at 350 nm. Adding Ho-TCA (52 mg) to a dichloromethane solution containing substrates and stirring for 12 h afforded new crystalline solids; the intensity was recorded at 435 nm, and excitation was at 350 nm. Solid-state cyclic voltammograms were measured by using a carbon-paste working electrode; a well-ground mixture of each bulk sample and carbon paste (graphite and mineral oil) was set in the channel of a glass tube and connected to a copper wire. A platinum-wire counter electrode and an Ag/AgCl reference electrode were used. Measurements were performed by using a three-electrode system in phosphate-buffered saline [PBS] at a scan rate of 50 mV s<sup>-1</sup>, in the range 0.5–1.1 V.

**Synthesis of Zn-BCIP1.** A mixture of 4,4',4''-tricarboxytriphenylamine ( $H_3TCA$ ; 94 mg, 0.25 mmol), Zn(NO<sub>3</sub>)<sub>2</sub>·6H<sub>2</sub>O (292 mg, 1 mmol) and *L*-BCIP (150 mg, 1 mmol) were dissolved in 15 mL mixed solvents of DMF and ethanol in a screw-capped vial. The resulting mixture was kept in an oven at 100 °C for 3 days. Crystals suitable for X-ray structural analysis were obtained after filtration. Yield: 60%. <sup>1</sup>H NMR (400 MHz, DMSO-*d*<sub>6</sub>/DCl):  $\delta = 9.10$  (s, 1H, imidazole ring), 7.92, 7.90 (d, 6H, Ph), 7.74–7.65 (t, 2H, imidazole ring), 7.15, 7.13 (d, 6H, Ph), 4.28–4.24 (m, 1H, CH<sub>2</sub>), 4.14–4.10 (m, 2H, CH<sub>2</sub> and pyrrole ring CH), 3.27–3.25 (m, 2H, pyrrole ring CH<sub>2</sub>), 1.80–1.64 (m, 4H, 2 × pyrrole ring CH<sub>2</sub>), 1.42 (s, 9H, tri-*tert*-butyl). Anal. Calcd for Zn<sub>2</sub>H<sub>2</sub>O(OH)(C<sub>21</sub>H<sub>12</sub>NO<sub>6</sub>)(C<sub>13</sub>H<sub>21</sub>N<sub>3</sub>O<sub>2</sub>): C, 51.60; H, 4.58; N, 7.08. Found: C, 51.54; H, 4.42; N, 7.10. FTIR (KBr pellet; cm<sup>-1</sup>): 3416 (w), 2975 (m), 2927 (m), 2893 (m), 1595 (m), 1392 (m), 1315 (m), 1275 (m), 1176 (m), 1090 (s), 1050 (s) cm<sup>-1</sup>.

**Synthesis of Zn-BCIP2.** A mixture of 4,4',4''-tricarboxytriphenylamine ( $H_3TCA$ ; 94 mg, 0.25 mmol), Zn(NO<sub>3</sub>)<sub>2</sub>·6H<sub>2</sub>O (292 mg, 1 mmol), and *D*-BCIP (150 mg, 1 mmol) were dissolved in 15 mL of mixed solvents of DMF and ethanol in a screw-capped vial. The resulting mixture was kept in an oven at 100 °C for 3 days. Crystals suitable for X-ray structural analysis were obtained after filtration. Yield: 65%. <sup>1</sup>H NMR (400 MHz, DMSO-*d*<sub>6</sub>/DCl):  $\delta = 9.14$  (s, 1H, imidazole ring), 7.92, 7.90 (d, 6H, Ph), 7.73–7.69 (t, 2H, imidazole ring), 7.15, 7.14 (d, 6H, Ph), 4.26–4.23 (m, 1H, CH<sub>2</sub>), 4.15–4.12 (m, 2H, CH<sub>2</sub> and pyrrole ring CH), 3.28–3.25 (m, 2H, pyrrole ring CH<sub>2</sub>), 1.85–1.66 (m, 4H, 2 × pyrrole ring CH<sub>2</sub>), 1.43 (s, 9H, tri-*tert*-butyl). Anal. Calcd for Zn<sub>2</sub>H<sub>2</sub>O(OH)(C<sub>21</sub>H<sub>12</sub>NO<sub>6</sub>)(C<sub>13</sub>H<sub>21</sub>N<sub>3</sub>O<sub>2</sub>): C, 51.60; H, 4.58; N, 7.08. Found: C, 51.74; H, 4.50; N, 7.21. FTIR (KBr pellet; cm<sup>-1</sup>): 3411 (w), 2974 (m), 2926 (m), 2893 (m), 1595 (m), 1390 (m), 1315 (m), 1282 (m), 1172 (m), 1109 (s), 1053 (s) cm<sup>-1</sup>.

**Synthesis of Zn-PYIs.** Zn-BCIP in DMF was heated at 165 °C using microwave irradiation for about 4 h. Yield: > 95%. <sup>1</sup>H NMR (400 MHz, DMSO-*d*<sub>6</sub>/DCl):  $\delta = 9.11$  (s, 1H, imidazole ring), 7.93, 7.91 (d, 6H, Ph), 7.74–7.69 (t, 2H, imidazole ring), 7.16, 7.14 (d, 6H, Ph), 4.25–4.23 (m, 1H, CH<sub>2</sub>), 4.15–4.13 (m, 2H, CH<sub>2</sub> and pyrrole ring CH), 3.21–3.17 (m, 2H, pyrrole ring CH<sub>2</sub>), 1.80–1.69 (m, 4H, pyrrole ring CH<sub>2</sub>). Anal. Calcd for Zn<sub>2</sub>H<sub>2</sub>O(OH)(C<sub>21</sub>H<sub>12</sub>NO<sub>6</sub>)(C<sub>8</sub>H<sub>13</sub>N<sub>3</sub>): C, 50.38; H, 4.08; N, 8.10. Found: C, 50.10; H, 4.06; N, 7.92. FTIR (KBr pellet; cm<sup>-1</sup>): 3416 (w), 1595 (m), 1560 (m), 1392 (m), 1315 (s), 1275 (m), 1176 (m).

**Synthesis of Ho-TCA.** A mixture of 4,4',4''-tricarboxytriphenylamine ( $H_3TCA$ ; 94 mg, 0.25 mmol) and Ho(NO<sub>3</sub>)<sub>3</sub>·6H<sub>2</sub>O (459 mg, 1 mmol) were dissolved in 15 mL of mixed solvents of DMF and ethanol in a screw-capped vial. The resulting mixture was kept in an oven at 100 °C for 3 days. Yellow block-shaped crystals were obtained after filtration. Yield: 70%. <sup>1</sup>H NMR (400 MHz, DMSO-*d*<sub>6</sub>/DCl):  $\delta = 7.93$ , 7.91 (d, 6H, Ph), 7.16–7.14 (m, 6H, Ph). Anal. Calcd for [Ho<sub>4</sub>(OH)<sub>4</sub>(OH)<sub>2</sub>(C<sub>21</sub>H<sub>12</sub>NO<sub>6</sub>)<sub>2</sub>(H<sub>2</sub>O)<sub>4</sub>·2H<sub>2</sub>O: C, 31.17; H, 2.62; N, 1.73. Found: C, 32.03; H, 1.91; N, 1.89. FTIR (KBr pellet; cm<sup>-1</sup>): 3442 (w), 1678 (m), 1589 (m), 1538 (m), 1504 (m), 1318 (m), 1273 (m), 1180 (m), 1104 (s), 1016 (s) cm<sup>-1</sup>.

**Single-Crystal X-ray Crystallography.** Intensities were collected on a Bruker SMART APEX CCD diffractometer with graphite-monochromated Mo K $\alpha$  radiation ( $\lambda = 0.71073$  Å) using the SMART and SAINT programs.<sup>72,73</sup> The structure was solved by direct methods and refined on  $F^2$  by full-matrix least-squares methods with SHELXTL version 5.1.<sup>74</sup> Non-hydrogen atoms of the ligand backbones were refined anisotropically. Hydrogen atoms within the ligand backbones

and the bridging hydroxyl group were fixed geometrically at calculated positions and allowed to ride on the parent non-hydrogen atoms. Crystallographic data for Zn-BCIP1, Zn-BCIP2, and Ho-TCA are given in Table 3.

**Table 3. Crystallographic Data for Zn-BCIP1, Zn-BCIP2, and Ho-TCA**

	Zn-BCIP1	Zn-BCIP2	Ho-TCA
empirical formula	C <sub>34</sub> H <sub>36</sub> N <sub>4</sub> O <sub>10</sub> Zn <sub>2</sub>	C <sub>34</sub> H <sub>36</sub> N <sub>4</sub> O <sub>10</sub> Zn <sub>2</sub>	C <sub>42</sub> H <sub>42</sub> Ho <sub>4</sub> N <sub>2</sub> O <sub>24</sub>
formula wt	791.45	791.45	1618.50
T/K	220	220	298
cryst syst	monoclinic	monoclinic	tetragonal
space group	P2 <sub>1</sub>	P2 <sub>1</sub>	P̄4 <sub>2</sub> c
a/Å	9.657(1)	9.789(1)	12.573(2)
b/Å	22.049(2)	22.293(3)	12.573(2)
c/Å	16.376(2)	16.533(2)	25.944(8)
β/deg	91.51(1)	91.75(3)	
V/Å <sup>3</sup>	3485.7(6)	3605.6(8)	4101.2(2)
Z	4	4	2
D <sub>calcd</sub> /g	1.504	1.455	1.311
μ/mm <sup>-1</sup>	1.439	1.391	3.869
no. of rflns collected	12 489	29 006	18 712
no. of unique rflns	7964	11 838	3611
R(int)	0.1123	0.1242	0.1220
F(000)	1624	1624	1536
R1 (I > 2σ) <sup>a</sup>	0.0760	0.0734	0.0664
wR2 (all data) <sup>b</sup>	0.1290	0.1544	0.1692
GOF	1.032	1.004	1.017

$${}^a R_1 = \sum |F_o| - |F_c| / \sum |F_o|, {}^b wR_2 = [\sum w(|F_o|^2 - |F_c|^2)^2]^{1/2} / \sum w(F_o^2)^{1/2}$$

For Zn-BCIP1 and Zn-BCIP2 crystals, hydrogen atoms of the water molecules and the hydroxyl groups were found from the different Fourier map but refined by using the riding model with the thermal parameter being fixed at 1.2 times of the oxygen atoms to which they are attached. Several bond distance constraints were used to aid refinement of the BCIP moiety.

For the Ho-TCA crystal, the geometrical constraints of idealized regular polygons were used for several disordered benzene rings, the C-C bond distance of the phenyl ring being 1.39 Å and the diagonal C-C distance of the phenyl ring being 2.78 Å.

**Typical Procedure for the Alkylation of Aldehydes.** *Catalysis Reactions with Zn-PYIs as Catalysts.* The quartz glass tube was purged with a stream of nitrogen, and 0.8 mL of dry THF was added via syringe, followed by the corresponding 1.5 mg of Zn-PYI (0.5 mol %; 1.9 μmol, 0.005 equiv), 66.0 μL of diethyl bromomalonate (0.385 mmol, 1.0 equiv), aldehyde (0.769 mmol, 2.0 equiv), and 90.0 μL of 2,6-lutidine (0.769 mmol, 2.0 equiv). The resultant mixture was degassed for 10 min by bubbling nitrogen through the reaction medium. After the reaction mixture was thoroughly degassed, the vial was sealed with Parafilm and placed approximately 8 cm from a 26 W fluorescent lamp source. After 24 h, the mixture was centrifuged on a Xiangyi TG16-WS centrifuge at 12 000 rpm for 5 min. The remaining solid was washed with THF (2 × 2 mL). The solid was dried in air prior to being reused. The supernatant solution was taken out via syringe and concentrated in vacuo. Yields were determined by <sup>1</sup>H NMR analysis. The reaction mixture was subjected to the workup protocol outlined in the general procedure and purified by flash chromatography using petroleum ether/Et<sub>2</sub>O (4/1) as the eluent to give the title compound as a colorless oil. The enantiomeric excess was determined according to the literature method:<sup>11</sup> 20 mg of the title compound was added to a mixture of 8.5 mg of (2S,4S)-(+)-pentanediol (>99% ee) and 1.5 mg of *p*-toluenesulfonic acid hydrate in CH<sub>2</sub>Cl<sub>2</sub> (1 mL). After consumption of the aldehyde was

complete (as judged by TLC analysis), the reaction mixture was concentrated in vacuo and the enantiomeric excess of the title compound was determined by the integration of the two <sup>1</sup>H NMR signals (both doublets) in CDCl<sub>3</sub> arising from the resultant diastereomeric acetals.

*Catalysis Reactions with Ho-TCA and MOF-150 as Catalysts.* A mixture of the catalyst (1.9 μmol, 0.005 equiv), 66.0 μL of diethyl bromomalonate (0.39 mmol, 1.0 equiv), 11.6 mg of L-/D-PYI (76.9 μmol, 0.2 equiv), aldehyde (0.77 mmol, 2.0 equiv), and 90.0 μL of 2,6-lutidine (0.77 mmol, 2.0 equiv) was degassed for 10 min by bubbling nitrogen through the reaction medium. After 24 h, the reaction mixture was subjected to the workup protocol outlined in the general procedure and purified by flash chromatography using petroleum ether/Et<sub>2</sub>O (4/1) as the eluent to afford the title compound as a colorless oil. The enantiomeric excess was also determined according to the above method.

## ■ ASSOCIATED CONTENT

### 📄 Supporting Information

Figures, tables, text, and CIF files giving crystal data, experimental details, and the catalysis results. This material is available free of charge via the Internet at <http://pubs.acs.org>.

## ■ AUTHOR INFORMATION

### Corresponding Author

\*E-mail: cyduan@dlut.edu.cn.

### Author Contributions

The manuscript was written through contributions of all authors. All authors have given approval to the final version of the manuscript.

### Notes

The authors declare no competing financial interest.

## ■ ACKNOWLEDGMENTS

We gratefully acknowledge the financial support from the NSFC (Nos. 21171029, 21025102, and 91122031).

## ■ REFERENCES

- Meeuwissen, J.; Reek, J. N. H. *Nat. Chem.* **2010**, *2*, 615–621.
- Cornils, B.; Herrmann, W. A.; Schlogl, R.; Wong, C. H. *Catalysis from A to Z*; Wiley-VCH: Weinheim, New York, 2000.
- Ciamician, G. *Science* **1912**, *36*, 385–394.
- Roth, H. D. *Angew. Chem., Int. Ed. Engl.* **1989**, *28*, 1193–1207.
- Ravelli, D.; Doni, D.; Fagnonia, M.; Albini, A. *Chem. Soc. Rev.* **2009**, *38*, 1999–2011.
- Hammarstrom, L.; Hammes-Schiffer, S. *Acc. Chem. Res.* **2009**, *42*, 1859–1860.
- Kalyanasundaram, K. *Coord. Chem. Rev.* **1982**, *46*, 159–244.
- Zeitler, K. *Angew. Chem., Int. Ed.* **2009**, *48*, 9785–9789.
- Narayanam, J. M. R.; Stephenson, C. R. J. *Chem. Soc. Rev.* **2011**, *40*, 102–113.
- Gust, D.; Moore, T. A.; Moore, A. L. *Acc. Chem. Res.* **2009**, *42*, 1890–1898.
- Nicewicz, D. A.; MacMillan, D. W. C. *Science* **2008**, *322*, 77–80.
- Vignola, N.; List, B. *J. Am. Chem. Soc.* **2004**, *126*, 450–451.
- Yoon, T. P.; Ischay, M. A.; Du, J. *Nat. Chem.* **2010**, *2*, 527–532.
- Xie, Z. G.; Wang, C.; deKrafft, K. E.; Lin, W. B. *J. Am. Chem. Soc.* **2011**, *133*, 2056–2059.
- Cherevatskaya, M.; Neumann, M.; Fuldner, S.; Harlander, C.; Kummel, S.; Dankesreiter, S.; Pfitzner, A.; Zeitler, K.; König, B. *Angew. Chem., Int. Ed.* **2012**, *41*, 4062–4066.
- Herrmann, J. -M. *Top. Catal.* **2005**, *34*, 49–65.
- Fox, M. A.; Dulay, M. T. *Chem. Rev.* **1993**, *93*, 341–357.
- Kitagawa, S.; Kitaura, R.; Noro, S. *Angew. Chem., Int. Ed.* **2004**, *43*, 2334–2375.
- Long, J. R.; Yaghi, O. M. *Chem. Soc. Rev.* **2009**, *38*, 1213–1214.

- (20) Farha, O. K.; Hupp, J. T. *Acc. Chem. Res.* **2010**, *43*, 1166–1175.
- (21) Yaghi, O. M.; O'Keefe, M.; Ockwig, N. W.; Chae, H. K.; Eddaoudi, M.; Kim, J. *Nature* **2003**, *423*, 705–714.
- (22) Ferey, G. *Chem. Soc. Rev.* **2008**, *37*, 191–214.
- (23) Chen, B.; Xiang, S.; Qian, G. *Acc. Chem. Res.* **2010**, *43*, 1115–1124.
- (24) Li, J. R.; Kuppler, R. J.; Zhou, H. C. *Chem. Soc. Rev.* **2009**, *38*, 1477–1504.
- (25) Lee, J. Y.; Farha, O. K.; Roberts, J.; Scheidt, K. A.; Nguyen, S. T.; Hupp, J. T. *Chem. Soc. Rev.* **2009**, *38*, 1450–1459.
- (26) Yoon, M.; Srirambalaji, R.; Kim, K. *Chem. Rev.* **2012**, *112*, 1196–1231.
- (27) Nickerl, G.; Henschel, A.; Grüninger, R.; Gedrich, K.; Kaskel, S. *Chem. Ingen. Tech.* **2011**, *83*, 90–103.
- (28) Corma, A.; García, H.; Xamena, F. X. L. *Chem. Rev.* **2010**, *110*, 4606–4655.
- (29) Farrusseng, D.; Aguado, S.; Pinel, C. *Angew. Chem., Int. Ed.* **2009**, *48*, 7502–7513.
- (30) Czaja, A. U.; Trukhan, N.; Müller, U. *Chem. Soc. Rev.* **2009**, *38*, 1284–1293.
- (31) Song, F.; Zhang, T.; Wang, C.; Lin, W. *Proc. R. Soc. A* **2012**, *468*, 2035–2052.
- (32) Li, B.; Zhang, Y.; Ma, D.; Li, L.; Li, G.; Li, G.; Shi, Z.; Feng, S. *Chem. Commun.* **2012**, *48*, 6151–6153.
- (33) Shimidzu, T.; Iyoda, T.; Koide, Y. *J. Am. Chem. Soc.* **1985**, *107*, 35–41.
- (34) Neckers, D. C.; Valdes-Aguilera, O. M. *Adv. Photochem.* **1993**, *18*, 315–394.
- (35) Wallentin, C. -J.; Nguyen, J. D.; Finkbeiner, P.; Stephenson, C. R. J. *J. Am. Chem. Soc.* **2012**, *134*, 8875–8884.
- (36) Tucker, J. W.; Zhang, Y.; Jamison, T. F.; Stephenson, C. R. J. *Angew. Chem., Int. Ed.* **2012**, *51*, 4144–4147.
- (37) Shih, H. W.; Vander Wal, M. N.; Grange, R. L.; MacMillan, D. W. C. *J. Am. Chem. Soc.* **2010**, *132*, 13600–13603.
- (38) Nagib, D. A.; Scott, M. E.; MacMillan, D. W. C. *J. Am. Chem. Soc.* **2009**, *131*, 10875–10877.
- (39) Conrad, J. C.; Kong, J.; Laforteza, B. N.; MacMillan, D. W. C. *J. Am. Chem. Soc.* **2009**, *131*, 11640–11641.
- (40) Allen, A. E.; MacMillan, D. W. C. *J. Am. Chem. Soc.* **2011**, *133*, 4260–4263.
- (41) Dang, D. B.; Wu, P. Y.; He, C.; Xie, Z.; Duan, C. Y. *J. Am. Chem. Soc.* **2010**, *132*, 14321–14323.
- (42) Luo, S. Z.; Mi, X. L.; Zhang, L.; Liu, S.; Xu, H.; Cheng, J. P. *Tetrahedron* **2007**, *63*, 1923–1930.
- (43) Lun, D. J.; Waterhouse, G. I. N.; Telfer, S. G. *J. Am. Chem. Soc.* **2011**, *133*, 5806–5809.
- (44) Deshpande, R. K.; Minnaar, J. L.; Telfer, S. G. *Angew. Chem., Int. Ed.* **2010**, *49*, 4598–4602.
- (45) Cohen, S. M. *Chem. Rev.* **2012**, *112*, 970–1000.
- (46) Rawal, V. H.; Cava, M. P. *Tetrahedron Lett.* **1985**, *26*, 6141–6144.
- (47) Ma, L.; Falkowski, J. M.; Abney, C.; Lin, W. *Nat. Chem.* **2010**, *2*, 838–846.
- (48) Fang, Q. R.; Zhu, G. S.; Jin, Z.; Ji, Y. Y.; Ye, J. W.; Xue, M.; Yang, H.; Wang, Y.; Qiu, S. L. *Angew. Chem., Int. Ed.* **2007**, *46*, 6638–6642.
- (49) Xu, W.; Peng, B.; Chen, J.; Liang, M.; Cai, F. *J. Phys. Chem. C* **2008**, *112*, 874–880.
- (50) Grigoras, M.; Vacareanu, L.; Ivan, T. *Rev. Roum. Chim.* **2011**, *56*, 411–417.
- (51) Zhao, H.; Yuan, W. Z.; Tang, L.; Sun, J. Z.; Xu, H.; Qin, A.; Mao, Y.; Jin, J. K.; Tang, B. Z. *Macromolecules* **2008**, *41*, 8566–8574.
- (52) Lee, E. Y.; Jang, S. Y.; Suh, M. P. *J. Am. Chem. Soc.* **2005**, *127*, 6374–6381.
- (53) Kavarnos, G. J. *Fundamentals of Photoinduced Electron Transfer*; VCH: New York, 1993.
- (54) Rehm, D.; Weller, A. *Isr. J. Chem.* **1970**, *8*, 259–271.
- (55) Oishi, S.; Furuta, N. *Chem. Lett.* **1978**, *7*, 45.
- (56) Lazarides, T.; McCormick, T.; Du, P.; Luo, G.; Lindley, B.; Eisenberg, R. *J. Am. Chem. Soc.* **2009**, *131*, 9192–9194.
- (57) Xiao, Y.; Cui, Y.; Zheng, Q.; Xiang, S.; Qian, G.; Chen, B. *Chem. Commun.* **2010**, *46*, 5503–5505.
- (58) Horike, S.; Dinca, M.; Tamaki, K.; Long, J. R. *J. Am. Chem. Soc.* **2008**, *130*, 5854–5855.
- (59) Banerjee, M.; Das, S.; Yoon, M.; Choi, H. J.; Hyun, M. H.; Park, S. M.; Seo, G.; Kim, K. *J. Am. Chem. Soc.* **2009**, *131*, 7524–7525.
- (60) Cho, S.-H.; Ma, B.; Nguyen, S. T.; Hupp, J. T.; Albrecht-Schmitt, T. E. *Chem. Commun.* **2006**, 2563–2565.
- (61) Fang, Q.-R.; Yuan, D.-Q.; Sculley, J.; Li, J.-R.; Han, Z. -B.; Zhou, H. -C. *Inorg. Chem.* **2010**, *49*, 11637–11642.
- (62) Hasegawa, S.; Horike, S.; Matsuda, R.; Furukawa, S.; Mochizuki, K.; Kinoshita, Y.; Kitagawa, S. *J. Am. Chem. Soc.* **2007**, *129*, 2607–2614.
- (63) Telfer, S. G.; Tajima, N.; Kuroda, R. *J. Am. Chem. Soc.* **2004**, *126*, 1408–1418.
- (64) An, H.; Wang, E.; Xiao, D.; Li, Y.; Su, Z.; Xu, L. *Angew. Chem., Int. Ed.* **2006**, *45*, 904–908.
- (65) Ma, L.; Abney, C.; Lin, W. *Chem. Soc. Rev.* **2009**, *38*, 1248–1256.
- (66) Wayner, D. D. M.; Dannenberg, J. J.; Griller, D. *Chem. Phys. Lett.* **1986**, *131*, 189–191.
- (67) Chae, H. K.; Kim, J.; Friedrichs, O. D.; O'Keefe, M.; Yaghi, O. M. *Angew. Chem., Int. Ed.* **2003**, *42*, 3907–3909.
- (68) O'Keefe, M.; Hyde, B. G. *Crystal Structures, 1: Patterns and Symmetry*; Mineralogical Society of America: Washington, DC, USA, 1996.
- (69) Lee, E. Y.; Jang, S. Y.; Suh, M. P. *J. Am. Chem. Soc.* **2005**, *127*, 6374–6381.
- (70) Spek, A. L. *PLATON99, A Multipurpose Crystallographic Tool*; Utrecht University, Utrecht, The Netherlands, 1999.
- (71) Dapperheld, S.; Steckhan, E.; Brinkhaus, K. H. G.; Esch, T. *Chem. Ber.* **1991**, *124*, 2557–2567.
- (72) *SMART Data collection software (version 5.629)*; Bruker AXS Inc., Madison, WI, 2003.
- (73) *SAINT, Data reduction software (version 6.45)*; Bruker AXS Inc., Madison, WI, 2003.
- (74) Sheldrick, G. M. *SHELX-97: Program for crystal structure analysis*; University of Göttingen, Göttingen, Germany, 1997.